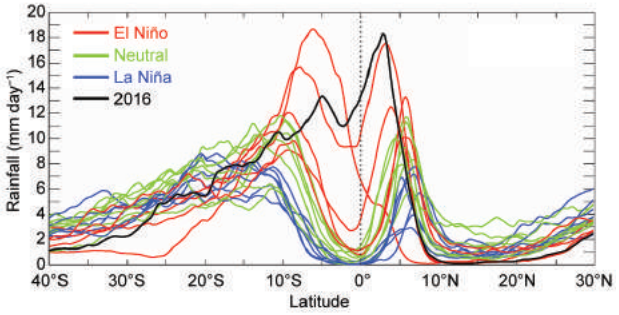

Fig. 4.13. CMORPH rainfall rate (mm day^{-1}) for Jan–Mar quarters for each year 1998 to 2016, averaged over the longitude sector 180°–150°W. The cross-sections are color-coded according to NOAA's ONI, except for 2016 (an El Niño quarter) shown in black.

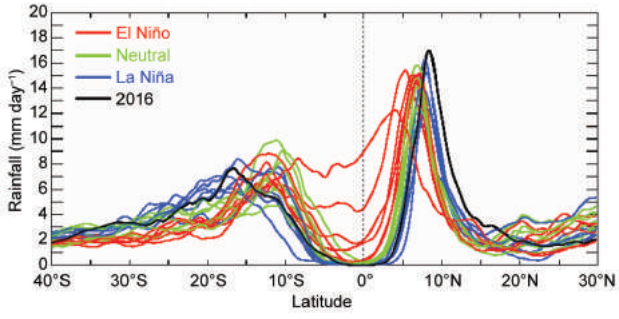

Fig. 4.14. CMORPH rainfall rate (mm day^{-1}) for Oct–Dec quarters, for each year 1998 to 2016, averaged over the longitude sector 180°–150°W. The cross-sections are color-coded according to NOAA's ONI, except for 2016 (a La Niña quarter) shown in black.

other year in the dataset (although close to the peak rainfall of January–March 2010, another El Niño season).

Not surprisingly, many off-equator islands in the Pacific experienced drought conditions during the early part of 2016 (Fig. 4.7). In the Northern Hemisphere, very dry conditions were experienced in January through April across much of Micronesia and into Hawaii, which is typical of the post-peak phase of a strong El Niño. The more northern islands fared worse than those closer to the equator. For example, April 2015 to March 2016 was the driest on record in parts of Palau (Koror; 7.3°N, 134.5°E), Yap State (Woleai; 7.4°N, 143.9°E), and the Marshall Islands (Jaluit; 6.0°N, 169.5°E), as reported in the May 2016 *Pacific ENSO Update* (www.weather.gov/media/peac/PEU/PEU_v22_n2.pdf).

In the Southern Hemisphere, rainfall was much lower than normal in many of the early months of the year as documented in more detail in Chapter 7. With the collapse of El Niño conditions in April–June, the two convergence zones behaved differently. The ITCZ showed a poleward displacement from May onwards (a La Niña signature), whereas the SPCZ remained unusually active for the time of year and maintained its equatorward displacement through the season (Fig. 4.12b). In July–September (Fig. 4.12c), the SPCZ convection had subsided and the ITCZ continued a more pronounced poleward displacement from its climatological position as weak La Niña conditions developed (see Section 4b).

In October–December (Figs. 4.12d, 4.14) the poleward displacement of the ITCZ was quite marked. Despite of the La Nina being categorized as weak, Fig. 4.14 suggests that the peak rainfall (near 8°N) in the 180°–150°W sector was the highest in the CMORPH dataset, with the ITCZ also displaced farther north between 10°N and 15°N than in any other year. The prolonged El Niño-related dry spell was finally broken in the Marshall Islands during October–December, with well-above-average rainfall in the northern atolls such as Kwajalein (8.7°N, 167.7°E).

2) Atlantic—A. B. Pezza and C. A. S. Coelho

The Atlantic ITCZ is a well-organized convective band that oscillates approximately between 5°–12°N during July–November and 5°N–5°S during January–May (Waliser and Gautier 1993; Nobre and Shukla 1996). Equatorial atmospheric Kelvin waves can modulate the ITCZ intraseasonal variability (Guo et al. 2014). ENSO and the southern annular mode (SAM) also influence the ITCZ on the interannual time scale (Münnich and Neelin 2005). The SAM is typically negative during El Niño events, but it was generally positive in 2016 despite the strong El Niño in 2015/16. This disconnect helps explain the mixed hemispheric response (L'Heureux et al. 2016).

In South America, extensive dry conditions occurred in southern Brazil in January. Meanwhile, excessive rain fell over the northeastern sector, which typically experiences rainfall deficits during El Niño events. Abnormally dry conditions returned for most of the tropical basin from February onwards as the El Niño dissipated (Figs. 4.15, 4.16). These dry conditions were associated in part with relatively warmer-than-normal waters in the western half of the North Atlantic sector (see Münnich and Neelin 2005). As a result, the Atlantic index, defined in Fig. 4.17 as the north–south sea surface temperature gradient, was moderately positive (Fig. 4.17a). The ITCZ tends to shift toward the warmer side of this gradient, and indeed it was generally north of its climatological position during 2016. The Southern Hemisphere lacked organized deep convection even during the sporadic southerly ITCZ bursts in early April (Fig. 4.17b). However, given the modest magnitude of the Atlantic

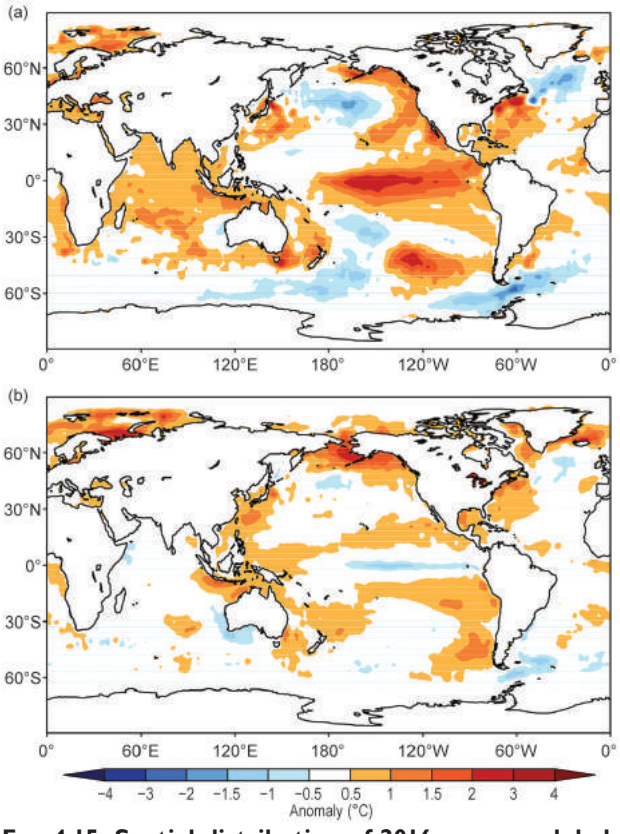

Fig. 4.15. Spatial distribution of 2016 average global SST anomalies (°C; Reynolds et al. 2002) for (a) Jan–Apr and (b) May–Dec.

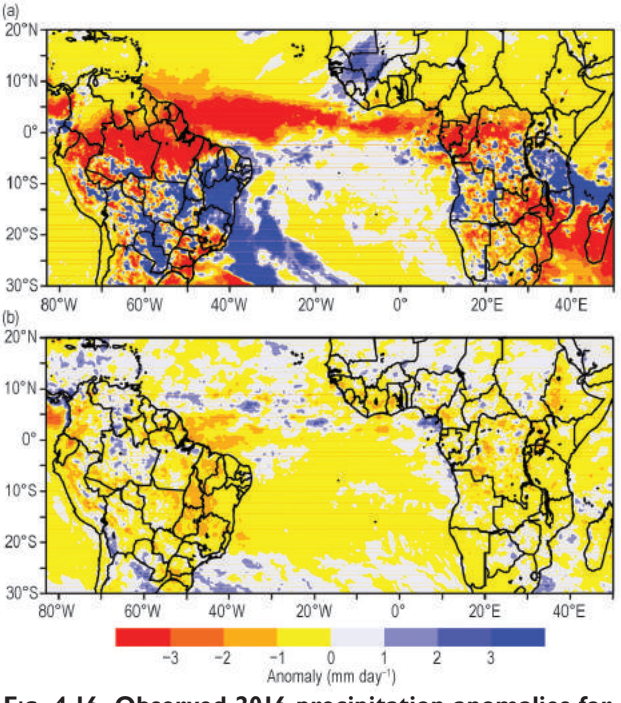

Fig. 4.16. Observed 2016 precipitation anomalies for (mm day^{-1}) tropical and subtropical South America during (a) Jan and (b) Feb–Dec 2016. Anomalies calculated based on a 1998–2015 climatology derived from CMORPH (Joyce et al. 2004).

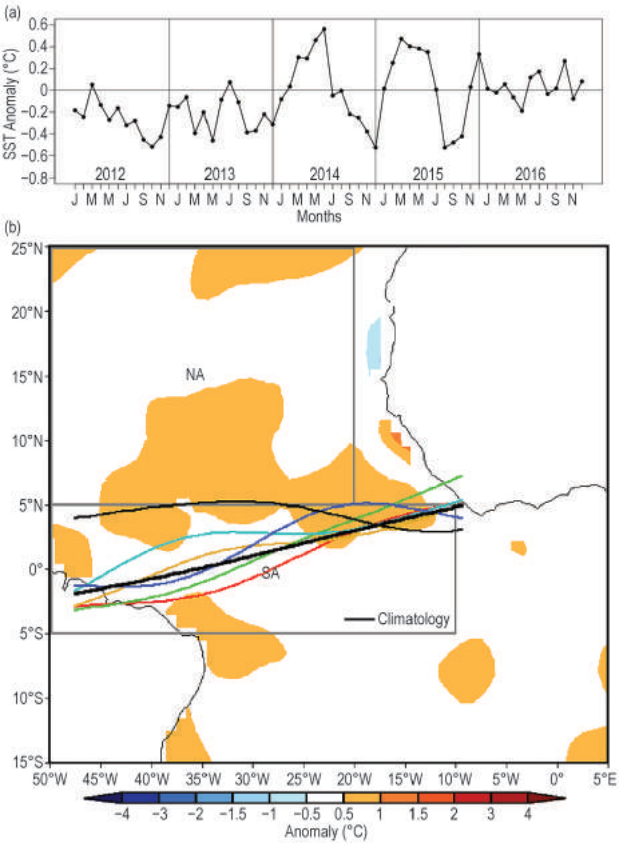

Fig. 4.17. (a) Monthly OISST (Smith et al. 2008) anomaly time series averaged over the South American sector (SA region, 10°–50°W, 5°S–5°N) minus the SST anomaly time series averaged over the North Atlantic sector (NA region, 20°–50°W, 5°–25°N) for the period 2012–16, forming the Atlantic index. The positive phase of the index indicates favorable conditions for enhanced Atlantic ITCZ activity. (b) Atlantic ITCZ position inferred from OLR (Liebmann and Smith 1996) during Apr 2016. The colored thin lines indicate the approximate position for the six pentads of the month. The black thick line indicates the Atlantic ITCZ climatological position for April. The SST anomalies for Apr 2016 based on the 1982–2015 climatology are shaded (°C). The two boxes indicate the areas used for the calculation of the Atlantic index in (a).

index, other factors likely contributed to the magnitude and extent of the drought.

Precipitation deficits across much of tropical and equatorial South America persisted after widespread drought within most of the Amazon and central Brazil, a feature already noted in Blunden and Arndt (2016) and in preceding editions of this chapter (Fig. 4.7). Persistently low vegetation health indices and reduced soil moisture most likely contributed to lowering the evapotranspiration and relative humidity, facilitating higher temperatures. This large-scale drought pattern extended into southeastern Brazil in recent years (Coelho et al. 2016a,b). Remarkably, this

dry pattern was already established before the latest El Niño event onset and remained in place after its termination. Recent research has attempted to assess if droughts in different parts of Brazil could be either part of a longer-term natural oscillation or attributed to anthropogenic forcing associated with climate change (Otto et al. 2015).

e. *Global monsoon summary*—B. Wang

The global monsoon is the dominant mode of annual variation of tropical–subtropical precipitation and circulation (Wang and Ding 2008) and thus a defining feature of seasonality and a major mode of variability of Earth's climate system. Figure 4.18 summarizes the monsoon rainfall anomalies for November 2015–October 2016—the global monsoon year that includes both the Southern Hemisphere summer monsoon from November 2015 to April 2016, and the Northern Hemisphere summer monsoon from May to October 2016.

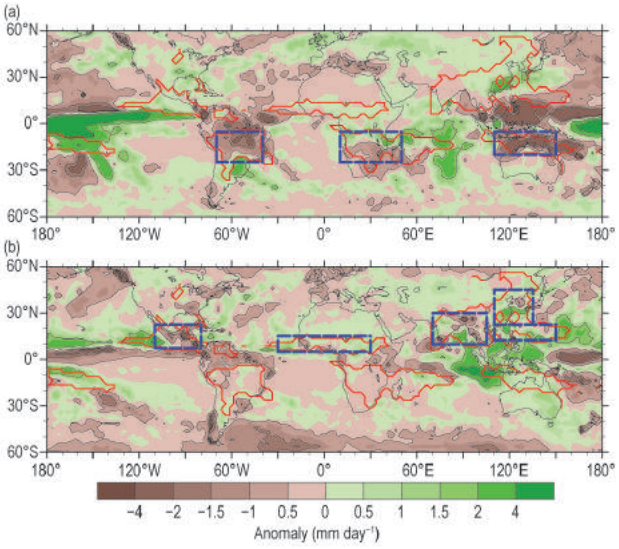

Fig. 4.18. Precipitation anomalies averaged for (a) Nov 2015–Apr 2016 and (b) May–Oct 2016. The red lines outline the global monsoon precipitation domain that is defined by (a) the annual range (local summer minus winter) precipitation exceeding 300 mm and (b) the summer mean precipitation exceeding 55% of the total annual precipitation amount (Wang and Ding 2008). Here the local summer denotes May–Sep for the NH and Nov–Mar for the SH. The precipitation indices for each regional monsoon are defined by the areal mean precipitation in the corresponding rectangular regions (dashed blue), which are highly correlated with the precipitation averaged over the corresponding real regional monsoon domains (Table 4.1 in Yim et al. 2014). The rainfall data were taken from the GPCP analysis from Jan 1979 to Aug 2016 (Huffman et al. 2009) and CMAP from Sep to Oct 2016 (Xie and Arkin 1997).

Table 4.1. (Modified from Yim et al. 2014). Definition of the regional summer monsoon circulation indices and their correlation coefficients (CCs) with the corresponding regional summer monsoon precipitation indices for the period 1979–2015. All circulation indices are defined by meridional shear of zonal winds at 850-hPa which measures the intensity (relative vorticity) of the monsoon toughs at 850 hPa except for the northern African (NAF) and East Asian (EASM). The NAF monsoon circulation index is defined by the westerly monsoon strength: U850 (0°–15°N, 60°–10°W) and the EASM circulation index is defined by the meridional wind strength: V850 (20°–40°N, 120°–140°E) which reflects the east-west thermal contrast between the Asian continent and western North Pacific. The precipitation indices are defined by the areal mean precipitation over the blue box regions shown in Fig. 4.18. The correlation coefficients were computed using monthly time series (148 summer months) (June to September (JJAS) in NH (1979–2015) and December to March (DJFM) in SH (1979/80–2015/16). The bolded numbers represent significance at 99% confidence level.

Region	Definition of the Circulation Index	CC
Indian (ISM)	U850 (5°–15°N, 40°–80°E) minus U850 (25°–35°N, 70°–90°E)	**0.73**
Western North Pacific (WNPSM)	U850 (5°–15°N, 100°–130°E) minus U850 (20°–35°N, 110°–140°E)	**0.76**
East Asian (EASM)	V850 (20°–40°N, 120°–140°E)	**0.73**
North American (NASM)	U850 (5°–15°N, 130°–100°W) minus U850 (20°–30°N, 110°–80°W)	**0.85**
Northern African (NAFSM)	U850 (0°–15°N, 60°–10°W)	**0.71**
South American (SASM)	U850 (5°–20°S, 70°–40°W) minus U850 (20°–35°S, 70°–40°W)	**0.80**
Southern African (SAFSM)	U850 (0°–15°S, 10°–40°E) minus U850 (10°–25°S, 40°–70°E)	**0.56**
Australian (AUSSM)	U850 (0°–15°S, 90°–130°E) minus U850 (20°–30°S, 100°–140°E)	0.89

The global land monsoon precipitation is strongly influenced by ENSO, especially the land areas of Asia, Australia, northern Africa, and Central America (Wang et al. 2012). From November 2015 to October 2016, the equatorial Pacific SSTs evolved from a peak phase of the strong El Niño 2015/16 to the weak La Niña in October 2016.

During Southern Hemisphere summer (November 2015–April 2016), correspond-

ing to the peak phase of the El Niño, the Southern Hemisphere summer monsoon precipitation was severely suppressed. Deficient rainfall prevailed over the Maritime Continent and Australian monsoon region (except for a narrow band along the equator), the ITCZ in the western and central Pacific, the South Pacific convergence zone, Brazil, and the western Atlantic ITCZ. On the other hand, enhanced precipitation occurred over the equatorial Pacific from 160°E to 100°W, central Indian Ocean, and southeastern China (Fig. 4.18a). The Southern Hemisphere summer monsoon was deficient, mainly due to the drought conditions over the Australian and South American monsoon regions.

During Northern Hemisphere summer (May–October 2016), the precipitation in the equatorial region tended to be reversed. Enhanced rainfall is found over the Maritime Continent, east Asian subtropical region, eastern equatorial Indian Ocean, and the ITCZ in the North Pacific. Meanwhile suppressed rainfall was seen in the equatorial Pacific from 150°E to 80°W, the central-western Indian Ocean, South Pacific convergence zone, and the North and Central American, Venezuelan, and South Asia monsoon regions (Fig. 4.18b).

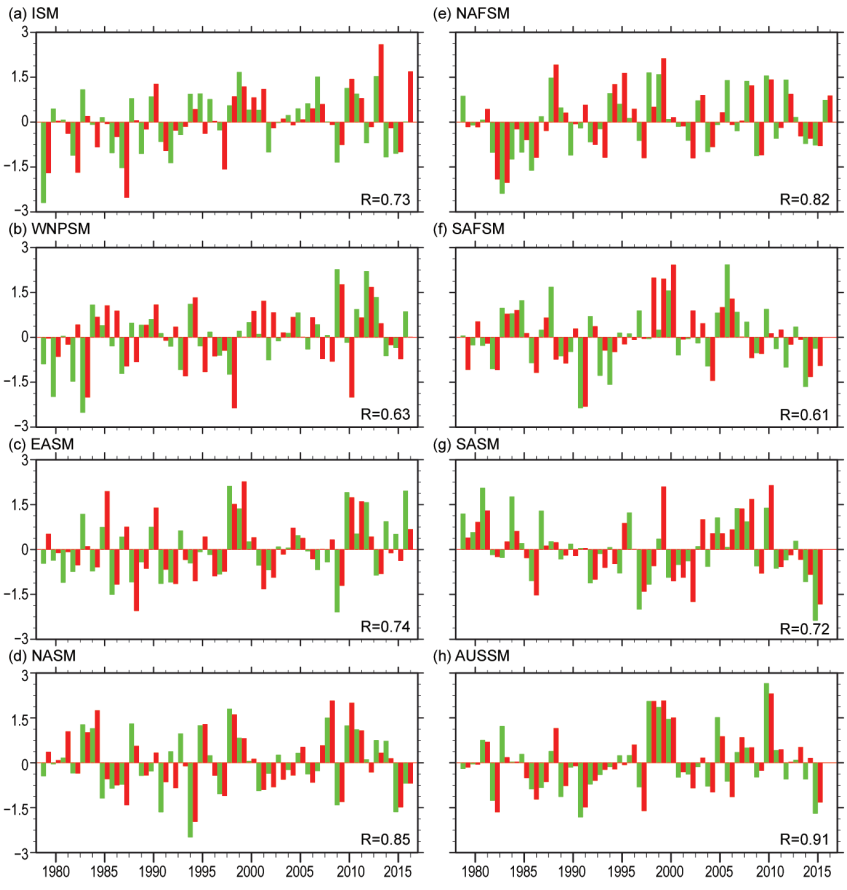

Fig. 4.19. Normalized summer mean precipitation (green) and circulation (red) indices in each of eight regional monsoons defined in Table 4.1. The indices are normalized by their corresponding std. dev. The numbers shown in the corner of each panels denote the correlation coefficient between seasonal mean precipitation and circulation indices. Here the summer denotes May–Oct for the NH and Nov–Apr for the SH. [Source: GPCP (Jan 1979–Aug 2016) and CMAP (Sep–Oct 2016).]

Figure 4.19 shows the time series of the monsoon precipitation and lower tropospheric circulation indices for each regional monsoon season. Note that the precipitation indices represent the total amount of precipitation over both land and ocean. The definitions of circulation indices for each monsoon region are shown in Table 4.1. The precipitation and circulation indices together represent the strength of each regional monsoon system. As discussed above, from November 2015 to April 2016 during the peak El Niño, all three Southern Hemisphere regional monsoons were weak and rainfall was deficient, especially, for the Australian and South American monsoons (Figs. 4.19f–h). During May to October, the North American summer monsoon, mainly over Central America and Venezuela, shows moderate negative anomalies (Fig. 4.19d); while the East Asian and northern African summer monsoon are stronger than normal (Figs. 4.19c,e). China experienced heavy flooding from south to north as reflected by the conspicuous positive May–October mean rainfall anomalies (Fig. 4.19c). Over India, the circulation index is high but the rainfall index is normal (Fig. 4.19a). The total strength of the Northern Hemisphere summer monsoon is slightly above normal. Note that these results pertain to the summer mean monsoon strength. Over the Indian and western North Pacific summer monsoon regions, there were large month-to-month fluctuations due to intraseasonal oscillations.

f. Tropical cyclones

1) Overview—H. J. Diamond and C. J. Schreck

The IBTrACS dataset comprises historical tropical cyclone (TC) best-track data from numerous sources around the globe, including all of the WMO Regional Specialized Meteorological Centers (RSMC; Knapp et al. 2010). IBTrACS represents the most complete compilation of global TC data and offers a unique opportunity to revisit the global climatology of TCs. Using IBTrACS data (Schreck et al. 2014) a 30-year average value for storms (from WMO-based RSMC numbers) is noted for each basin.

The tallying of the global TC numbers is challenging and involves more than simply adding up basin totals, because some storms cross TC basin boundaries, some TC basins overlap, and multiple agencies are involved in tracking and categorizing the TCs.

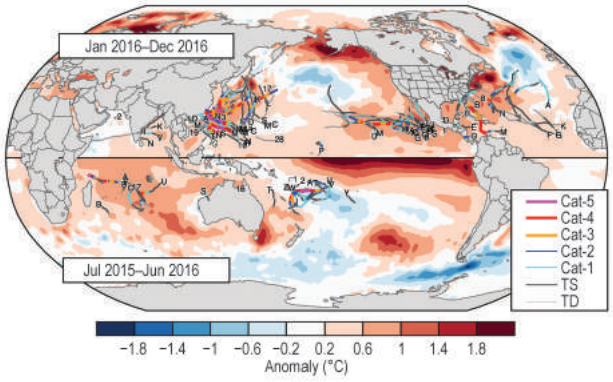

Fig. 4.20. Global summary of TC tracks with respect to SST anomalies (°C) for the 2016 TC season.

Compiling the activity using preliminary IBTrACS data over all seven TC basins (Fig. 4.20), the 2016 season (2015/16 in the Southern Hemisphere) had 93

SIDEBAR 4.1: RECORD-SETTING NORTH ATLANTIC HURRICANE MATTHEW—P. J. KLOTZBACH

The 2016 North Atlantic hurricane season was the first above-average Atlantic hurricane season based on the NOAA definition since 2012. The most notable storm of 2016, in terms of intensity, longevity, damage, and fatalities was Hurricane Matthew. Matthew formed from a tropical wave as it neared the Lesser Antilles, and over the course of the following 12 days, it cut a path of devastation across portions of Hispaniola, Cuba, the Bahamas, and then along the U.S. southeast coast before finally becoming post-tropical. In this sidebar, several of Hurricane Matthew's most notable meteorological records are highlighted. All statistics for Matthew listed are from the operational b-decks, which are utilized to initialize the numerical model guidance on tropical cyclones in real-time every six hours. The b-decks are available at http://ftp.nhc.noaa.gov/atcf/btk. Historical statistics are calculated from the HURDAT2 database, which provides six-hourly estimates of historical Atlantic tropical cyclone wind speeds, pressures, and locations since 1851 (Landsea and Franklin 2013).

After being named a tropical storm on 28 September, Matthew steadily intensified. Beginning 30 September, however, Matthew rapidly intensified, reaching category 5 strength with one-minute sustained winds of 140 kt (72 m s^{-1}) on 1 October (Fig. SB4.1). In the 24 hours leading up to reaching category 5 strength, Matthew intensified by 70 kt (36 m s^{-1}), the third fastest 24-hour intensification in the Atlantic basin on record, trailing only the 24-hour rapid intensification rates of Hurricane Wilma (2005) and Hurricane Felix (2007). Matthew was also the first category 5 hurricane in the Atlantic basin since Hurricane Felix (2007). In addition, it reached category 5

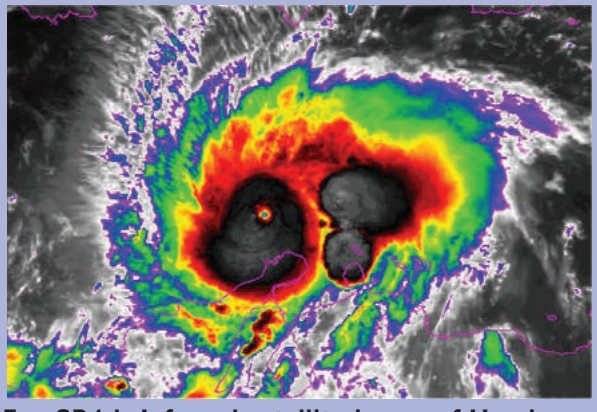

Fig. SB4.1. Infrared satellite image of Hurricane Matthew from GOES-East at near peak intensity at 0800 UTC 1 Oct 2016.

intensity at an unusually low latitude for an Atlantic hurricane: Matthew became a category 5 at 13.3°N, the lowest latitude Atlantic category 5 hurricane on record, breaking the old record of 13.7°N set by Hurricane Ivan (2004).

While Matthew only maintained category 5 intensity for 12 hours, it was notable for its longevity at category 4–5 strength, especially during the latter part of the Atlantic hurricane season. Matthew was a category 4–5 hurricane for 102 hours in October, the longest an Atlantic hurricane has maintained that intensity on record during October. Due to its intense nature and slow movement, Matthew generated the most ACE (Bell et al. 2000) by any Atlantic tropical cyclone on record in the eastern Caribbean (≤20°N, 75°–60°W). Matthew was also a major hurricane for over seven days, the

named storms (wind speeds ≥ 34kt or 17 m s^{-1}), which is above the 1981–2010 average of 82 TCs (Schreck et al. 2014), but eight fewer than the 2015 total of 101 TCs (Diamond and Schreck 2016). The 2016 season also featured 58 hurricanes/typhoons/cyclones (HTC; wind speeds ≥ 64kt or 33 m s^{-1}), which is above the 1981–2010 average of 46 HTCs (Schreck et al. 2014). Twenty storms reached major HTC status (wind speeds ≥ 96kt or 49 m s^{-1}), which is near the long-term average of 21. In Sections 4f2–4f8, the 2016 seasonal activity is described and compared to the historical record for each of the seven WMO-defined hurricane basins. For simplicity, all counts are broken down by the United States' Saffir–Simpson scale. Figure 4.20 depicts the overall picture of global TCs during 2016. The North Atlantic hurricane season was above normal (Section 4f2), and both the central and eastern North Pacific hurricane seasons were well above normal (Section 4f3).

Globally, four storms achieved Saffir–Simpson category 5 during the year (four fewer than in 2015, and three fewer than in 2014): (a) Hurricane Matthew in the North Atlantic; (b) Supertyphoon Meranti in the western North Pacific; (c) Cyclone Fantala in the South Indian Ocean; and (d) Tropical Cyclone Winston in the Southwest Pacific. Matthew was the costliest hurricane ($10 billion U.S. dollars in damages) to strike the U.S. since Hurricane Sandy in 2012. Sidebar 4.1 recounts several of the records that Matthew broke. Supertyphoon Meranti, with maximum sustained winds of 165 kt (85 m s^{-1}), was the most intense tropical cyclone of the year globally. Sidebar 4.2 describes an unusual situation where Taiwan was impacted by four major typhoons, including

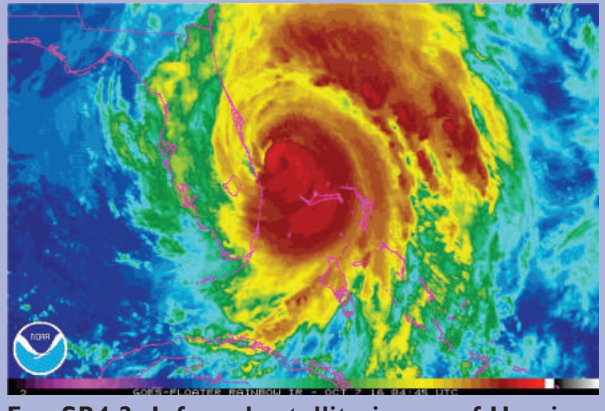

Fig. SB4.2. Infrared satellite image of Hurricane Matthew from GOES-East near its closest approach to the east coast of Florida at 0445 UTC 7 Oct 2016.

longest-lived major hurricane to form in the Atlantic after 25 September on record.

Matthew made landfall in Haiti as a category 4 hurricane on 4 October, becoming the first category 4 storm to hit Haiti since Cleo in 1964. While the final death toll from Matthew in Haiti may never be fully known, the National Hurricane Center reports (www.nhc.noaa.gov/data/tcr/AL142016_Matthew.pdf) that Matthew was responsible for 585 direct fatalities across four countries with 546 of those occurring in Haiti. Matthew then made landfall in Cuba as a category 4 hurricane, becoming the first category 4 hurricane to hit Cuba since Ike in 2008. Next, Matthew struck the Bahamas, battering the island chain also as a category 4 hurricane. In the process, Matthew became the first hurricane in the historical record (back to 1851) to make landfall at category 4 intensity in Haiti, Cuba, and the Bahamas.

Matthew tracked within 100 miles of the east coast of Florida (Fig. SB4.2), threatening to break the record-long U.S. landfalling major hurricane drought that has existed since October 2005 when Hurricane Wilma made landfall (Hart et al. 2016). It eventually made landfall along the central South Carolina coast as a weakening category 1 hurricane. Matthew was the first hurricane to make landfall in South Carolina since Gaston in 2004 and the first to make landfall north of Georgia during October since Hazel in 1954.

While the center of Matthew remained offshore of both Florida and Georgia, storm surge and heavy rainfall caused significant flooding in northeast Florida and along the entire coastline of Georgia. The eastern portions of both South and North Carolina suffered significant damage due to the combination of storm surge and heavy rainfall. Matthew was responsible for nearly 50 deaths in the United States, and total insured and uninsured damage from the storm was estimated at approximately $10 billion (U.S. dollars; www.ncdc.noaa.gov/billions).

Matthew was certainly the most notable storm in the Atlantic in 2016, as it was the longest-lived hurricane, the most intense storm, and the most damaging and destructive storm of the season. To put its longevity and intensity into perspective, while Matthew was one of 15 storms that formed in the Atlantic in 2016, it singlehandedly was responsible for 35% of the total amount of ACE generated by Atlantic tropical cyclones in 2016.

Meranti—three of which struck during September alone. Several other Saffir–Simpson category 3 and 4 intensity level systems during 2016 had major impacts: (1) Hurricane Nicole in the North Atlantic; (2) Typhoons Chaba, Haima, Malakas, Megi, Lionrock, Nepartik, and Nock-Ten in the western North Pacific; and (3) Typhoon Victor in the Southwest Pacific. Also noteworthy was that 2015/16 was the first year since the onset of the satellite era in 1970 that no major HTCs were observed in the Australian basin.

2) Atlantic basin—G. D. Bell, E. S. Blake, C. W. Landsea, C. Wang, J. Schemm, T. Kimberlain, R. J. Pasch, and S. B. Goldenberg

(i) Seasonal activity

The 2016 Atlantic hurricane season produced 15 named storms, of which 7 became hurricanes and 4 became major hurricanes (Fig. 4.21a). The HURDAT2 30-year (1981–2010) seasonal averages (as embodied in IBTrACS) are 11.8 tropical (named) storms, 6.4 hurricanes, and 2.7 major hurricanes (Landsea and Franklin 2013).

The 2016 seasonal ACE value (Bell et al. 2000) was about 148% of the 1981–2010 median (92.4×10^4 kt^2; Fig. 4.21b), which is above NOAA's lower threshold (120% of the median) for an above-normal season (see www.cpc.ncep.noaa.gov/products/outlooks). Based on this ACE value, combined with above-average numbers of named storms, hurricanes, and major hurricanes, NOAA officially classified the 2016 Atlantic hurricane season as above normal. This was the first above-normal season since 2012, producing more than 2.5 times the average ACE value of the last three seasons 2013–15.

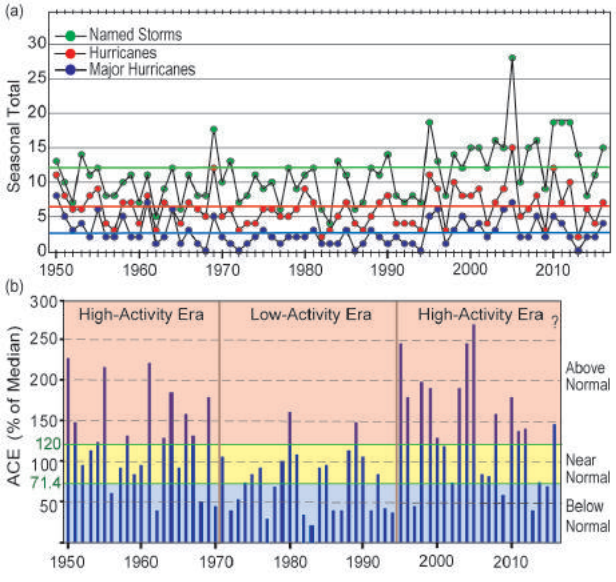

Fig. 4.21. Seasonal Atlantic hurricane activity during 1950–2016. (a) Numbers of named storms (green), hurricanes (red), and major hurricanes (blue), with 1981–2010 seasonal means shown by solid colored lines. (b) ACE index expressed as percent of the 1981–2010 median value. ACE is calculated by summing the squares of the 6-hourly maximum sustained surface wind speed (knots) for all periods while the storm is at least tropical storm strength. Red, yellow, and blue shadings correspond to NOAA's classifications for above-, near, and below-normal seasons, respectively. Vertical brown lines separate high- and low-activity eras. High and low activity eras are defined per Goldenberg et al. (2001).

(ii) Storm tracks and landfalls

The Atlantic hurricane main development region (MDR; green boxed region in (Fig. 4.22a) spans the tropical Atlantic Ocean and Caribbean Sea between 9.5° and 21.5°N (Goldenberg and Shapiro 1996; Goldenberg et al. 2001; Bell and Chelliah 2006). A main delineator between more- and less-active Atlantic hurricane seasons is the number of hurricanes and major hurricanes that first become named storms within the MDR during the peak months (August–October; ASO) of the hurricane season.

During ASO 2016, eight named storms formed in the MDR (Fig. 4.20), with five becoming hurricanes and four of those becoming major hurricanes. Three hurricanes were observed over the Caribbean Sea, a region with only one hurricane during the past three seasons (2013–15). The MDR activity during 2016 is comparable to the above-normal season averages for the MDR of 8.2 named storms, 6.0 hurricanes, and 3.0 major hurricanes. In contrast, the MDR averages for the last three seasons were 5.0 named storms with 2.3 becoming hurricanes and 1.0 becoming a major hurricane. These values are near the MDR averages for seasons that are not classified as above normal: 3.3 named storms, 2.0 hurricanes, and 1.0 major hurricanes.

Another feature of the 2016 season was that two major hurricanes (Matthew and Nicole) formed during October and accounted for more than 50% of the seasonal ACE value. The October 2016 ACE value was more than 50% larger than that of any other October since at least 1981 (Schreck et al. 2014).

The 2016 Atlantic hurricane season included a sharp increase in the number of landfalling storms compared to the last three seasons. In the United States, five named storms made landfall, including two hurricanes: Tropical Storm Bonnie and Hurricane Matthew struck South Carolina; Tropical Storms Colin and Julia, and Hurricane Hermine made landfall in Florida. This was the most U.S. landfalling storms since 2008 (six storms). Hermine was not only the first landfalling hurricane in the United